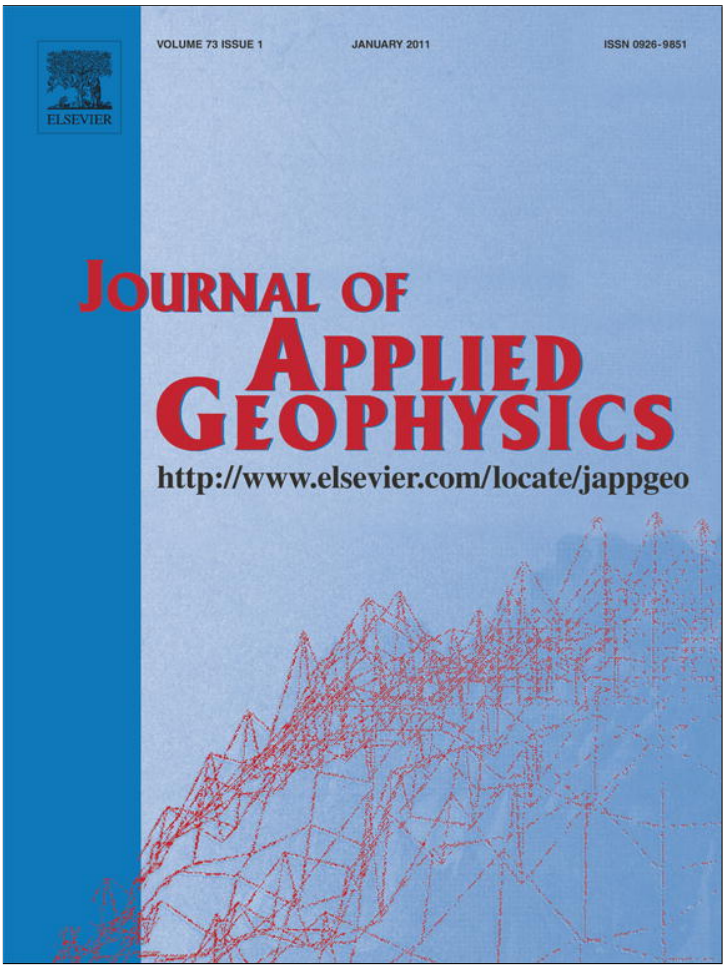

(This is a sample cover image for this issue. The actual cover is not yet available at this time.)

Journal of Applied Geophysics 74 (2011) 175–184

Contents lists available at ScienceDirect

Journal of Applied Geophysics

journal homepage: www.elsevier.com/locate/jappgeo

Model track studies on fouled ballast using ground penetrating radar and multichannel analysis of surface wave

P. Anbazhagan [a,*,1], Su Lijun [b,c,1], Indraratna Buddhima [c,2], Rujikiatkamjorn Cholachat [c]

[a] Department of Civil Engineering, Indian Institute of Science, Bangalore, 560012, India
[b] School of Civil Engineering, Xi'an University of Architecture & Technology, Xi'an Shaanxi 710055 PR China
[c] Faculty of Engineering, University of Wollongong, Wollongong, NSW 2522, Australia

ARTICLE INFO

Article history:
Received 26 March 2010
Accepted 8 May 2011
Available online xxxx

Keywords:
Ballast
Fouling
GPR
Seismic surface-wave survey
Shear wave velocity

ABSTRACT

Ballast fouling is created by the breakdown of aggregates or outside contamination by coal dust from coal trains, or from soil intrusion beneath rail track. Due to ballast fouling, the conditions of rail track can be deteriorated considerably depending on the type of fouling material and the degree of fouling. So far there is no comprehensive guideline available to identify the critical degree of fouling for different types of fouling materials. This paper presents the identification of degree of fouling and types of fouling using non-destructive testing, namely seismic surface-wave and ground penetrating radar (GPR) survey. To understand this, a model rail track with different degree of fouling has been constructed in Civil engineering laboratory, University of Wollongong, Australia. Shear wave velocity obtained from seismic survey has been employed to identify the degree of fouling and types of fouling material. It is found that shear wave velocity of fouled ballast increases initially, reaches optimum fouling point (OFP), and decreases when the fouling increases. The degree of fouling corresponding after which the shear wave velocity of fouled ballast will be smaller than that of clean ballast is called the critical fouling point (CFP). Ground penetrating radar with four different ground coupled antennas (500 MHz, 800 MHz, 1.6 GHz and 2.3 GHz) was also used to identify the ballast fouling condition. It is found that the 800 MHz ground coupled antenna gives a better signal in assessing the ballast fouling condition. Seismic survey is relatively slow when compared to GPR survey however it gives quantifiable results. In contrast, GPR survey is faster and better in estimating the depth of fouling.

1. Introduction

Railways are the massive means of transport in all countries to carry goods as well as passengers. The important component in railway is rail track, which consists of two parallel steel rails, anchored on perpendicular sleepers, these rails and sleepers being placed on a foundation. The foundation is normally compressed soil, on top of which a bed of ballast (aggregates) to distribute the load from the sleepers to the capping layers and formation soils. A ballast bed performs two major roles in the railway network, i.e., drainage and load bearing capacity. Rail ballast comprises of uniformly-graded coarse aggregates, produced from crushing locally available rocks such as granite, basalt, limestone, slag or gravel. During the operation, ballast fouling can take place due to ballast breakdown, infiltration of other materials from ballast surface or from base of ballast layer by filling of its voids. Major fouling reported worldwide is attributed to the breakdown of ballast (fine ballast), outside contamination by coal dust from trains carrying coal and due to soil intrusions from the base. Fouled ballast can cause the following major problems.

i. Reduction in vertical (including uplift), lateral and longitudinal forces applied to the sleepers to retain the track in its required position.
ii. Decrease in resilient modulus/strength and energy absorption capacity
iii. Reduction in the voids space thereby leading to a considerable decrease in the movement of particles through the ballast.
iv. Poor drainage of water falling onto track
v. Vegetation growth in the rail track
vi. Increased noise level and
vii. Inadequate electrical resistance between rails.

Therefore evaluation of the degree of fouling is necessary to ensure the optimum maintenance cycle thereby increasing track stability. The measures which are widely used to determine the fouling quantities are Fouling Index, Percentage of Fouling, D-Bar method,

* Corresponding author. Tel.: +91 80 22932467; fax: +91 80 23600404.
E-mail addresses: anbazhagan@civil.iisc.ernet.in, anbazhagan2005@gmail.com, anbupriyan2003@yahoo.com (P. Anbazhagan), lijun@uow.edu.au (S. Lijun), indra@uow.edu.au (I. Buddhima), cholacha@uow.edu.au (R. Cholachat).
URL: http://civil.iisc.ernet.in/~anbazhagan/ (P. Anbazhagan).
[1] The first two authors have contributed equally to this paper.
[2] Tel.: +61 2 4221 3046.

0926-9851/$ – see front matter © 2011 Elsevier B.V. All rights reserved.
doi:10.1016/j.jappgeo.2011.05.002

Percentage Void Contamination and Relative Ballast Fouling Ratio. The first three measures are commonly used; the fourth one is introduced by Queensland Rail (Feldman and Nissen, 2002) and the last one was recently developed by Indraratna et al.(2011). These methods are laboratory based and require field sampling and testing, which are normally carried out by digging trenches at even intervals; however these processes require a lot of resources (i.e. time, money and man power). Non-destructive testing of ground penetrating radar, infra-red imaging, seismic survey and electrical resistivity are popular among others for fouling identification in the field (Anbazhagan et al., 2010). However none of the testing method has been quantified to assess the critical degree of fouling. To address these issues, this study presents 1) construction technique of model rail tracks with various degree of fouling for different types of fouling materials, 2) estimation of low strain shear wave velocity using seismic surface-wave survey, 3) identification of degree of fouling and ballast thickness by ground penetrating radar, 4) comparing the seismic surface-wave survey and GPR results, and 5) identification of critical degree of fouling based on the low strain shear wave velocity.

2. Materials and fouling measures

A model track was composed of four different fouling conditions, namely, clean ballast (CB), ballast fouled with fine ballast/pulverized rock (FB), ballast fouled with coal (C) and ballast fouled with clayey sand (CS). The gradation of the clean ballast was selected within the upper and lower gradations recommended by the Australian Standards (AS, 2758.7, 1996). The gradation of materials used in this study is shown in Fig. 1; clean ballast are course aggregates having a minimum particle size of 9.5 mm and maximum size of 62 mm. Fouling materials of pulverized rock, coal and clayey sand have a maximum particle size of 9.5 mm.

Fouling conditions are measured using five methods.These are Fouling Index, Percentage of Fouling, D-Bar method, Percentage Void Contamination and Relative Ballast Fouling Ratio. The Fouling Index (FI) can be calculated by the dry weight of fine particles. The Fouling Index is the sum of the percentage of fine particles passing the 4.75 mm sieve and the 75 micron sieve. D-Bar is a number that represents the weighted geometric average of particle sizes passing through grading sieves from a full sample. A fresh ballast has a typical D-Bar = 36.0 mm and ballast is deemed to need replacement when D-Bar = 10 mm. The percentage of fouling (% fouling) is the ratio of the dry weight of material passing 9.5 mm sieve to the dry weight of total sample (Selig and Waters, 1994). The FI, D-bar and percentage of fouling provide the same result although the specific gravities are totally different. To overcome this issue, volume based method has been developed by Feldman and Nissen(2002) called Percentage of Void Contamination (PVC). PVC is a ratio between void volume in the ballast particles and volume of fouling particles passing 9.5 mm sieve. This was further modified to consider the difference in specific gravity of various materials such as clay and coal. Relative Ballast Fouling Ratio (R_{bf}) can be defined as a weighted ratio of the dry weight of fouling particles (passing 9.5 mm sieve) to the dry weight of ballast (particles retaining on 9.5 mm sieve) by Indraratna et al.(2011).

The relative ballast fouling ratio (R_{bf}) can be defined as:

$$R_{bf} = \frac{M_f \times \frac{G_{sb}}{G_{sf}}}{M_b} \times 100\% \quad (1)$$

where, M_f and M_b, and G_{sf} and G_{sb} are mass and specific gravities of fouling materials and ballast respectively. Fig. 2 shows the relationships between FI and percentage of fouling and R_{bf}. In this study the fouled sections were built by varying the percentage of fouling and the Relative Ballast Fouling Ratio. The ratio between the weight of clean ballast and fouling materials was chosen to result in an R_{bf} of 10% (% fouling of 4.94 and 8.75 for coal and clayey sand), 25% (% fouling of 11.5, 19.35 and 20 for coal, clayey sand and fine ballast), and 50% (% fouling of 20.64 and 32.43 for coal and clayey sand). The thickness of fouled part of the ballast and the R_{bf} for each section are listed in Table 1. Design and construction of the model track and preparation of fouled sections are discussed in the next section.

3. Construction of model track

A section of full scale railway track has been built in the Civil Engineering Laboratory, University of Wollongong for this study. The model track has all of the components of a railway track system, including subgrade, capping layer, and ballast (clean/fouled). No loading tests will be carried out on the model track. Hence the box was constructed with two layers of plywood boards. The outer layer is of 18 mm thick plywood boards and the inner layer is of 12 mm thick marine plywood boards which are water resistant. At the bottom of the box, PVC pipes were placed above the membrane for saturating the track for further studies. The box was strengthened with timber bracings to increase the stiffness of the side walls. Fig. 3 shows several photos of the box showing almost all of its details. The internal dimensions of the box are 4.76 m in length, 3.48 m in width, and 0.79 m in height. The track is formed by a subgrade layer of clayey sand, a capping layer of road base material and a ballast layer. The thicknesses of these layers were 15 cm for the subgrade, 15 cm for the capping layer and 49 cm for the ballast, respectively. Geotextile and

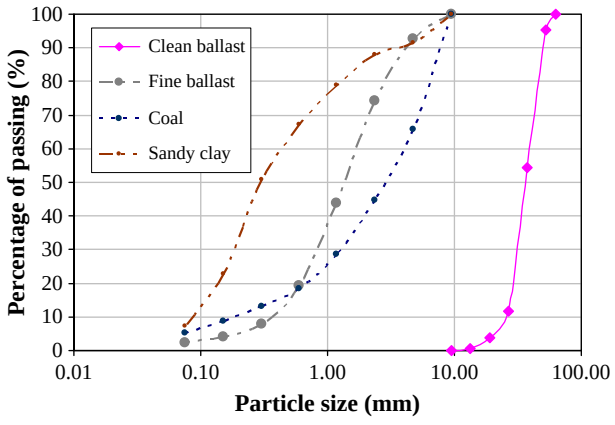

Fig. 1. The gradation of materials used to construct model track.

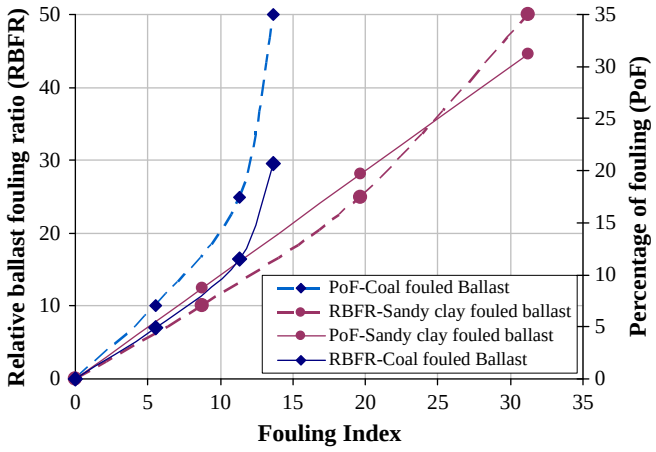

Fig. 2. Relationships between fouling index to percentage fouling and relative ballast fouling ratio for coal and sandy clay fouled ballast.

Table 1
Details for the sub-sections.

	Types of fouling	Thickness of fouled part (cm)	Relative ballast fouling ratio
Section 1	Coal	15	10%
Section 2	Coal	20	25%
Section 3	Ballast breakdown	27	25%
Section 4	Clayey sand	27	25%
Section 5	Clayey sand	20	10%
Section 6	Clean	N/A	N/A
Section 7	Clayey sand	20	50%
Section 8	Clean	N/A	N/A
Section 9	Coal	20	50%

Geogrids were placed between the subgrade and capping layer. Radar Detectable Geotextile was placed on top of the capping layer at the right side of the box along the longitudinal direction to highlight the interface between the ballast and the capping layer. Fig. 4a and b shows the cross section across and along the model track. All the dimensions in the graphs are in centimeters. The subgrade and capping were compacted and combined using a handheld vibrating compactor. Even though sections show up to top of rail, in this study MASW and GPR surveys were carried out before placing the sleeper and rails i.e. the total section height is 57 cm.

The clean and fouled ballast were placed layer by layer having a thickness of 4–6 cm and compacted using handheld vibrating plate. During compaction, plywood boards were inserted between 2 sections as partitions to secure a distinct vertical interface between adjacent sections. A layer of Geotextile was placed between adjacent sections to prevent fouling materials flowing from one section to another especially when watering the ballast. Two long timber bars with notches were used to fix the partitions. Clean sections of ballast (6 and 8) were built by compacting equal layers using a hand-held vibrating plate. The dense clean ballast in section 8 was built by using more layers than in section 6. The fouled sub-sections were prepared by following two different methods. From sections 1 to 5, the fouling materials were added to the top of clean ballast before the compaction. During the preparation, a layer of clean ballast was firstly placed in the section, and then the corresponding fouling material calculated according to a certain R_{bf} value (Table 1) and spread uniformly on the ballast surface. After that, the ballast together with the fouling material was compacted using a hand-held vibrating plate. For sections 7 and 9, by considering the volume of fouling materials, the ballast and fouling materials were mixed together using a concrete mixer and then compacted in the sections layer by layer as above.

4. Seismic surface-wave survey

A number of seismic methods have been proposed for near-surface characterization and measurement of shear wave velocity using a great variety of testing configurations, processing techniques, and inversion algorithms. The most widely used techniques are Spectral Analysis of Surface Waves (SASW) and Multichannel Analysis of Surface Waves (MASW). The SASW method has been used for subsurface investigation for several decades (Al-Hunaidi, 1992; Ganji et al., 1997; Nazarian et al., 1983; Stokoe et al., 1994; Tokimatsu, 1995). In SASW method, the spectral analysis was conducted on a surface wave generated by an impulsive source and recorded by a pair of receivers. MASW is the improved new technique by incorporating a multichannel analysis of surface waves using active sources (Park et al., 1999; Xia et al., 1999; Xu et al., 2006). The MASW has been found to be a more efficient method for unraveling the shallow subsurface properties (Anbazhagan and Sitharam, 2008a; Park et al., 1999; Zhang et al., 2004). MASW is increasingly being applied to earthquake geotechnical engineering for seismic microzonation and site response studies (Anbazhagan and Sitharam, 2008b; Anbazhagan and

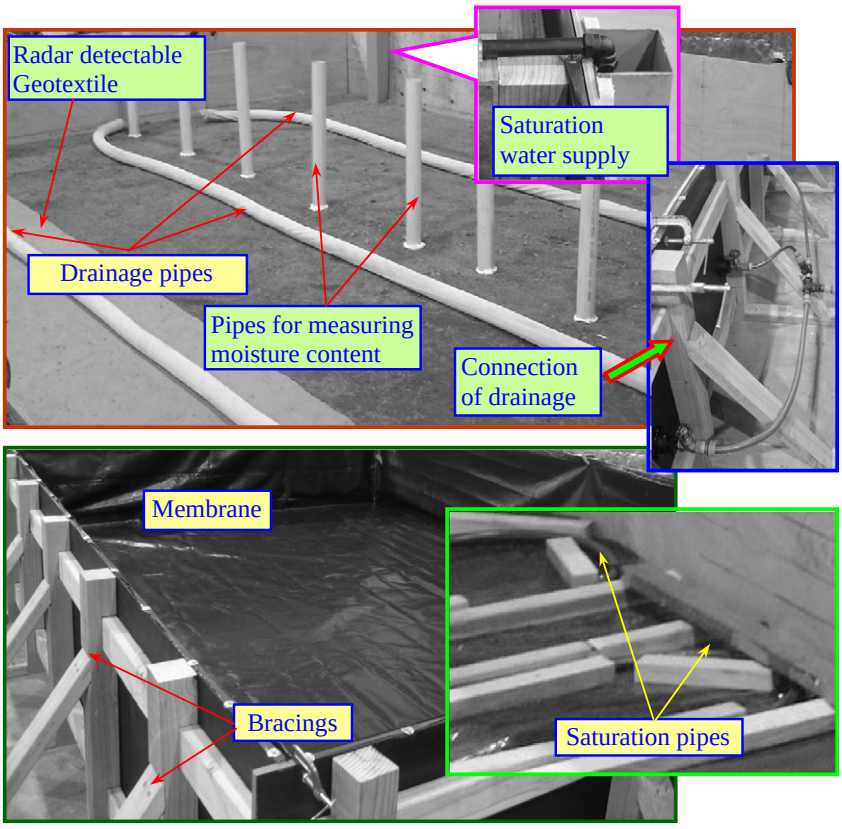

Fig. 3. Details of the model track.

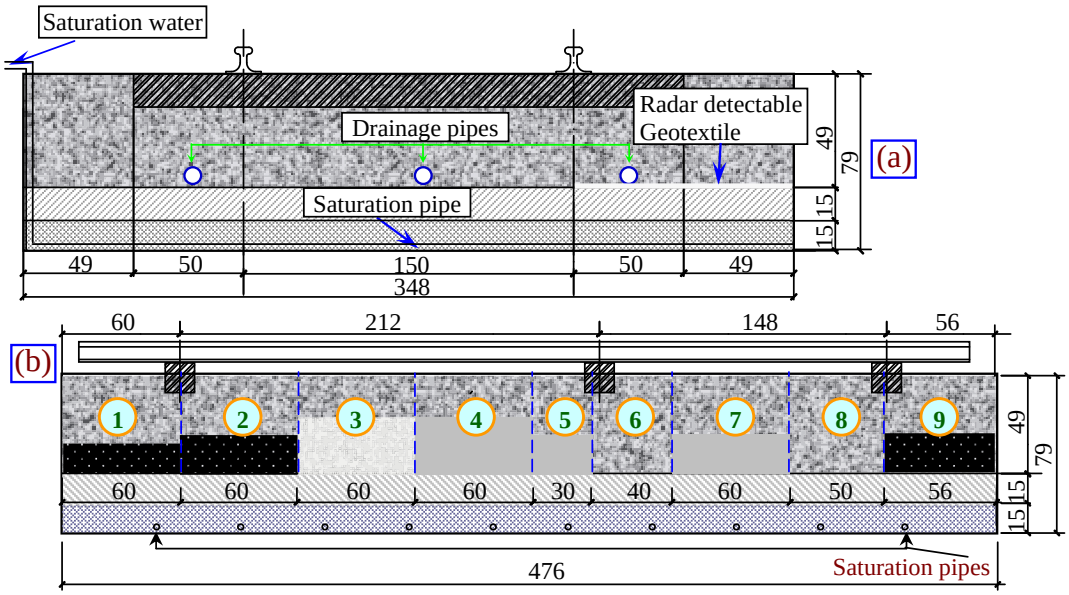

Fig. 4. Schematic diagrams of the model track: (a) cross section across the rail direction and (b) longitudinal section along rail direction (dimensions: cm).

Sitharam, 2008c; Anbazhagan and Sitharam, 2009). In particular, the MASW is used in geotechnical engineering for the measurement of shear wave velocity and dynamic properties (Sitharam and Anbazhagan, 2008; Anbazhagan and Sitharam, 2008d), identification of subsurface material boundaries and spatial variations of shear wave velocity (Anbazhagan and Sitharam, 2009).

MASW system consisting of 24 channels SmartSeis seismograph with 12 geophones of 10 Hz capacity was used. The seismic waves were created by impulsive source of 1 kg sledge hammer with 70 mm ×70 mm size aluminum plate with a number of shots. MASW survey was carried out by arranging 12 geophones parallel to the y axis along sections 1–9 (Fig. 4b). Different source to receiver distance and geophone spacing are investigated, and a good signal was obtained for a geophone spacing of 0.25 m and source to first receiver spacing of 0.5 m. This configuration was used to survey all the sections, and was similar to hard material (pavement) mapping field configuration (Anbazhagan and Sitharam, 2008d). Each section was surveyed three times and the seismic signals were recorded at a sampling interval of 0.125 ms and record length of 256 ms (Anbazhagan et al., 2010).

4.1. Dispersion curve and shear wave velocity

A dispersion curve is generally displayed as a function of phase velocity versus frequency. Phase velocity can be calculated from the linear slope of each component on the swept-frequency record. The shorter wavelengths are sensitive to the physical properties of surface layers (Xia et al., 1999). For this reason, a particular mode of surface wave will possess a unique phase velocity for each unique wavelength, leading to the dispersion of the seismic signal. For a multi-layered subsurface model, Rayleigh-wave dispersion curves can be calculated by Knopoff's method (Schwab and Knopoff, 1972). Rayleigh-wave phase velocity, c_{Rj}, is determined by a characteristic equation F in its nonlinear, implicit form:

$$F\left(f_j, c_{Rj}, v_s, v_p, \rho, h\right) = 0 (j = 1, 2, \ldots\ldots, m) \quad (2)$$

where f_j is the frequency, in Hz; c_{Rj} is the Rayleigh-wave phase velocity at frequency f_j; $v_s = (v_{s1}, v_{s2}, \ldots, v_{sn})^T$ is the S-wave velocity vector, with v_{si} the shear-wave velocity of the ith layer; n is the

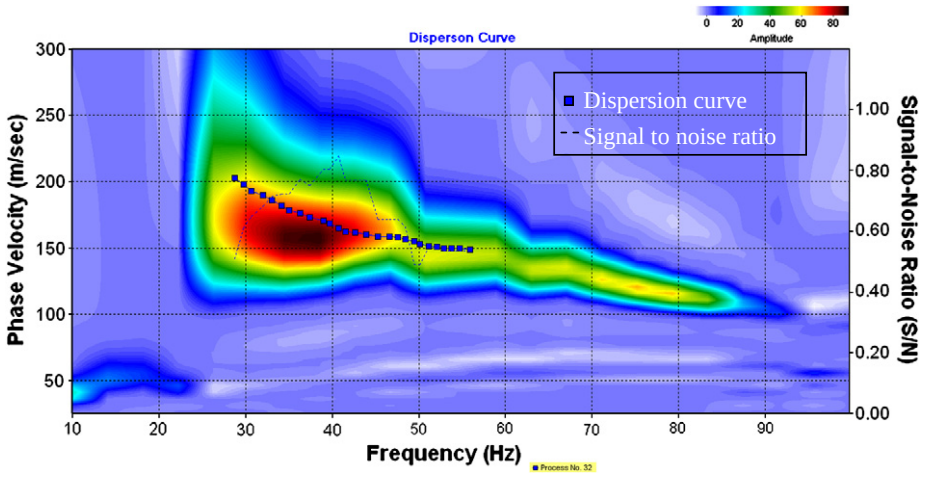

Fig. 5. Dispersion curve of ballast sections.

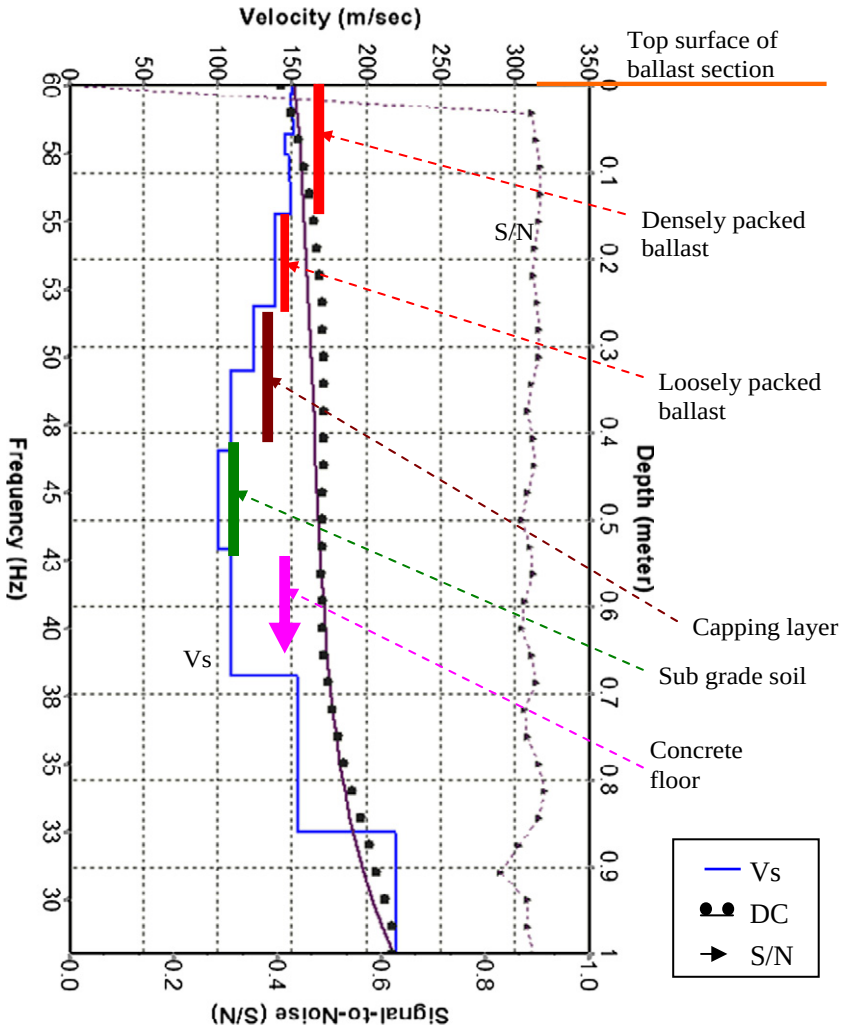

Fig. 6. A typical shear wave velocity (Vs) of section 8 with sectional profile. Legend Vs — shear wave velocity, Department of Civil Engineering — Dispersion curve and S/N — signal to noise ratio.

number of layers; $v_p = (v_{p1}, v_{p2},\ldots, v_{pn})^T$ is the compressive *P*-wave velocity vector, with v_{pi} the *P*-wave velocity of the *i*th layer; $\rho = (\rho_1, \rho_2, \ldots, \rho_n)^T$ is the density vector, with ρ_i the density of the *i*th layer; and $h = (h_1, h_2,\ldots, h_{n-1})^T$ is the thickness vector, with h_i the thickness of the *i*th layer. Given a set of model parameters (v_s, v_p, ρ, and h) and a specific frequency (f_j), the roots of Eq. (2) are the phase velocities. If the dispersion curve consists of *m* data points, a set of *m* equations in the form of Eq. (1) can be used to find phase velocities at frequencies f_j ($j = 1, 2,\ldots,m$) using the bisection method (Press et al., 1992); (Xia et al., 1999). In this study, only the fundamental mode is considered. The lowest analyzable frequency in this dispersion curve is around 10 Hz and highest frequency is 90 Hz. A typical dispersion curve along with signal amplitude and signal to noise ratio is shown in Fig. 5.

Shear wave velocity can be derived from inverting the dispersive phase velocity of the surface (Rayleigh and/or Love) wave (Aki and Richards, 1980; Dorman and Ewing, 1962; Mari, 1984; Xia et al., 1999). Shear wave velocity profile was calculated using an iterative inversion process that requires the dispersion curve developed earlier as input. A least-squares approach allows automation of the process (Xia et al., 1999). *S*-wave velocities of each layer can be represented as the elements of a vector $\mathbf{x}$ of length *n*, or $\mathbf{x} = [v_{s1}, v_{s2}, v_{s3},\ldots, v_{sn}]^T$. Similarly, the measurements (data) of Rayleigh-wave phase velocities at *m* different frequencies can be represented as the elements of a vector $\mathbf{b}$ of length *m*, or $\mathbf{b} = [b_1, b_2, b_3,\ldots, b_m]^T$. Since the model $\mathbf{c}_R$ [Eq. (2)] is a nonlinear function, Eq. (1) must be linearized by Taylor-series expansion to employ the matrix theory:

$$J\Delta X = \Delta b \tag{3}$$

where $\Delta\mathbf{b} = \mathbf{b} - \mathbf{c}_R(\mathbf{x}_0)$ and is the difference between measured data and model response to the initial estimation, in which $\mathbf{c}_R(\mathbf{x}_0)$ is the model response to the initial *S*-wave velocity estimates, $\mathbf{X}_0$; $\Delta\mathbf{X}$ is a

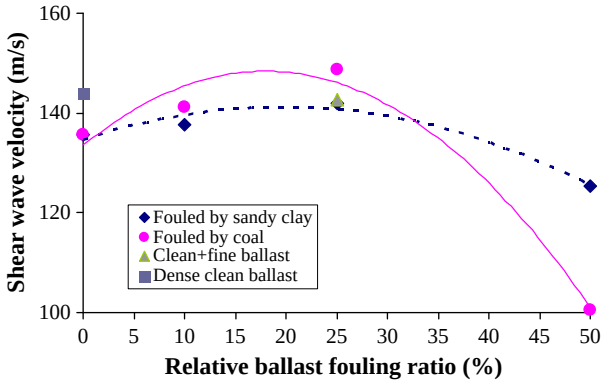

Fig. 7. Shear wave velocity of clean and fouled ballast.

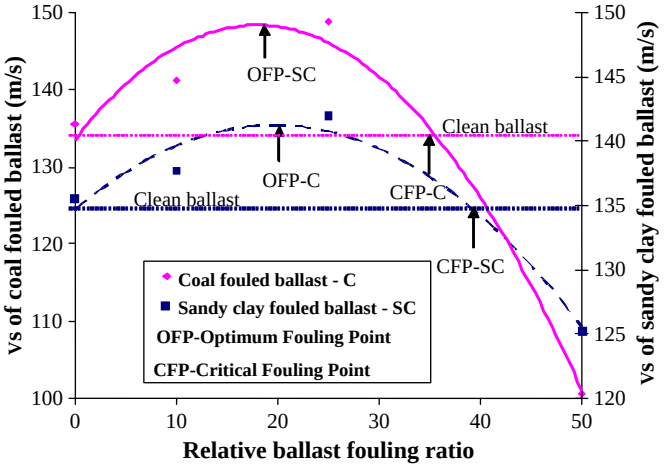

Fig. 8. Optimum and critical degree of fouling for sandy clay and coal fouled ballast.

modification of the initial estimation; and **J** is the Jacobian matrix with m rows and n columns ($m>n$). The elements of the Jacobian matrix are the first-order partial derivatives of $\mathbf{c}_R$ with respect to S-wave velocities. Since the number of data points contained in the dispersion curve is generally much larger than the number of layers used to define the subsurface ($m>n$), Eq. (2) is usually solved by optimization techniques. The objective function can be defined as

$$\Phi = ||J\Delta X - \Delta b||_2 W||J\Delta X - \Delta b||_2 + \alpha||\Delta X||_2^2 \quad (4)$$

where $||||_2$ is the l_2-norm length of a vector, α is the damping factor, and **W** is a weighting matrix. This is a constrained (weighted) least-squares problem. More details about the sensitivity of each parameter and calculation with respective examples are detailed in (Xia et al., 1999). Shear wave velocities of each location were inverted from respective dispersion curves. Typical shear wave velocity profile obtained for section 8 is shown in Fig. 6 and the interpretation will be presented in the next section. Ballast thickness is obtained from MASW by using 20 layer models, which are comparable with model section layers.

4.2. Clean and fouled ballast V_s

Shear wave velocities for sections 1–9 were determined by averaging three sets of data, having a standard deviation of less than 9. The study shows that the average shear wave velocity of clean ballast (sections 6 and 8) varies from 125 to 155 m/s for the density range of 1.59 t/m^3 to 1.66 t/m^3, which is similar to the ballast shear wave velocity, measured using the resonant column test by Bei(2005). Fig. 6 shows the typical shear wave velocity along with the cross section of section 8. The top layer has an average shear wave velocity (V_s) of about 148 m/s and it corresponds to clean ballast having a bulk density of 1.66 t/m^3. An average V_s of 135 m/s corresponds to the second layer of clean ballast section having a bulk density of 1.59 t/m^3. The average V_s of 115 m/s and 103 m/s corresponds to the capping layer and sub-grade layer below the ballast layer. After the sub-grade, the V_s values increase because of the concrete floor underneath the model track. In general, the average shear wave velocity of clean ballast is above 125 m/s and that of fouled ballast is above 80 m/s. It is also observed that there is a distinct difference between clean and fouled ballast shear wave velocity with respective layers within the same section. To further discuss the effects of the degree of fouling on shear properties, the relative ballast fouling ratio has been used. Fig. 7 shows the shear wave velocity of nine sections versus relative ballast fouling ratio. Shear wave velocity of the clean ballast increases when fouling materials are added up to a certain degree of fouling, and after that the shear wave velocity of fouled ballast is lower than the clean ballast. For a lower degree fouling, the shear wave velocity of coal fouled ballast is slightly more than that of clayey sand fouled ballast. However, a higher degree of coal fouled fouling gives a smaller shear wave velocity.

The observation of a higher shear wave velocity for less fouled may be attributed to particle size and the specific gravity of the coal. During mixing in the concrete mixer, the coal particles may break down, which can result in the lower shear wave velocity of coal fouled ballast when compared to ballast fouled by clayey sand. In section 3, ballast fouled by crushed rock shows a similar shear wave velocity to clayey sand fouled ballast in section 4.

4.3. Results and discussions

The shear wave velocity of fouled ballast initially increases and reaches maximum values, and then starts decreasing. Based on this study, it is observed that after a particular degree of fouling the shear wave velocity of fouled ballast decreases with the increase in the degree of fouling. The point corresponding to the largest shear wave velocity caused by ballast fouling can be called as the optimum fouling point (OFP). Beyond this peak point, the shear wave velocity decreases considerably. Fig. 8 shows the variation of shear wave velocity with the relative ballast fouling ratio. The OFP for clayey sand fouled ballast is in the range of 20% and OFP for coal fouled ballast is between 18% in terms of relative ballast fouling ratio. Even though the

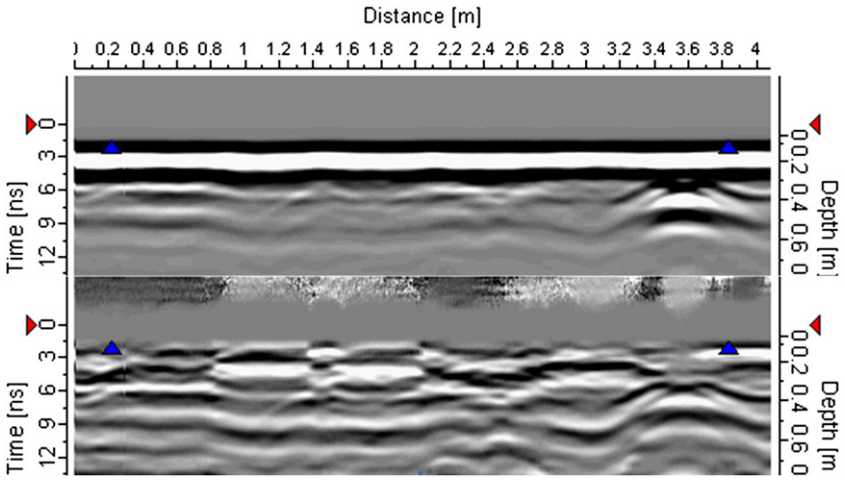

Fig. 9. Comparison between raw (top) and processed (bottom) GPR data from the 500 MHz antenna.

shear wave velocity of fouled ballast decreases after the OFP, it is still greater than the shear wave velocity of clean ballast, which means that the track may have sufficient resilient during this period, until it reaches a particular degree of fouling. However, limited studies are available to confirm this result. The shear wave velocity of fouled ballast reduces below the shear wave velocity of clean ballast; degree of fouling corresponding to this point can be defined as critical fouling point (CFP). Finer materials will be dominating thereby fouling beyond this point may be not acceptable in terms of strength and bearing capacity of track. Fig. 8 also shows the critical fouling point of clayey sand fouled ballast and coal fouled ballast. It is interesting to note that coal fouled ballast reaches the critical fouling point before clayey sand fouled ballast. This model track study shows that seismic surface-wave survey is more useful to identify not only the degree of fouling but also the type of fouling materials with shear wave velocity using multi layer models. For unknown field condition, determining depth of fouled ballast using seismic survey has to be further verified. Seismic surface-wave survey is time consuming when compare to GPR but results are quantifiable.

5. Ground penetrating radar survey

GPR is an electromagnetic sounding technique that is employed to investigate shallow sub-surface which have contrasting electrical properties (Daniels, 2004; Gallaghera et al., 1999). The GPR operates by transmitting short electromagnetic waves into the subsurface and recording and displaying the reflected energy. The data obtained from GPR testing is the time domain waveform representing the electromagnetic energy transmitted from the antenna and reflected off subsurface boundaries back to the antenna (Sussmanna et al., 2003). An examination of the reflected radar waveforms enables an interpretation of the material and/or structure under investigation

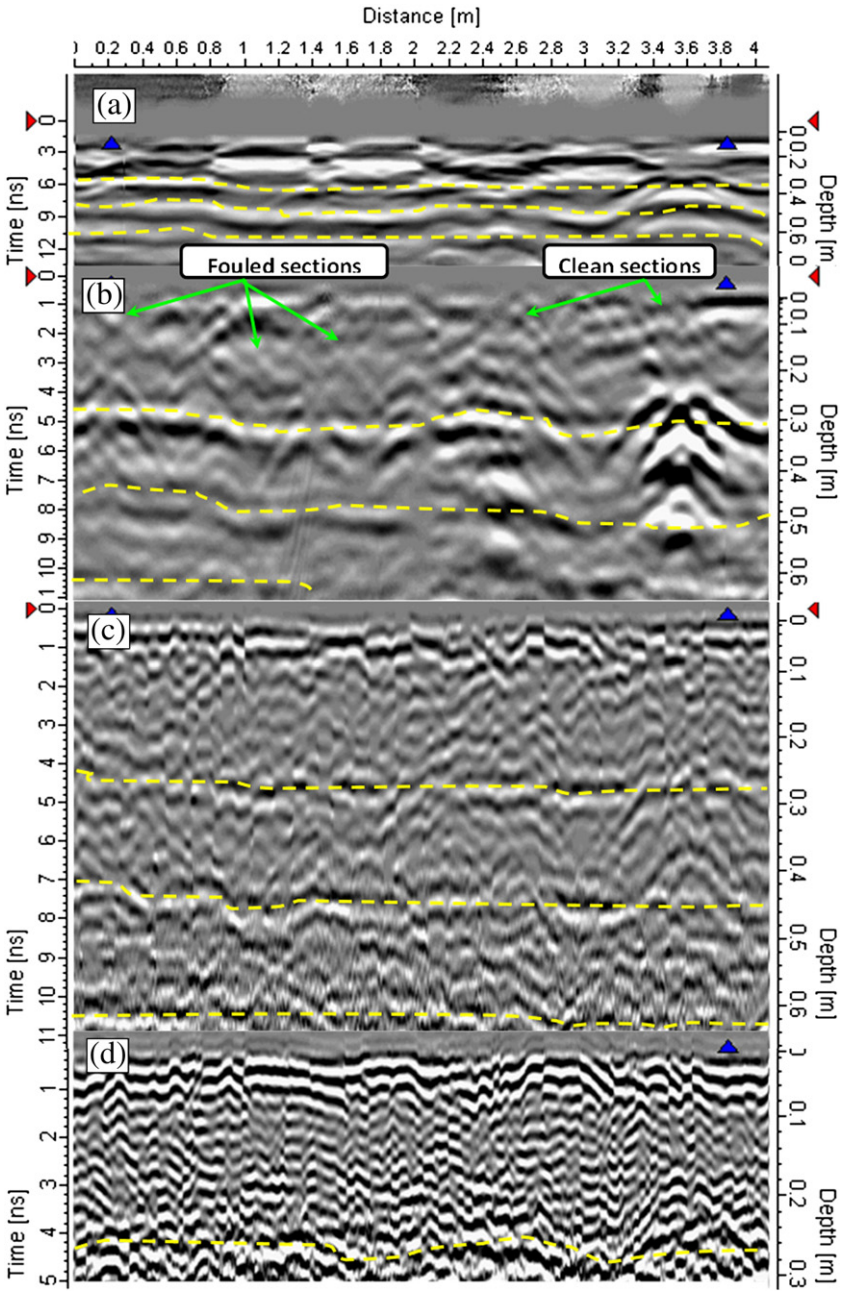

Fig. 10. Comparison between processed GPR data from different antennas: a, b, c and d shows the processed signal with respect to antenna frequency of 500 MHz, 800 MHz, 1.6 GHz and d 2.3 GHz.

(Clark et al., 2001). In radar survey, two kinds of velocity measurements can be carried out depending on whether the antenna offset is fixed or can be raised. Wide angle (WA) reflection or common midpoint (CMP) measurements provide the data necessary for calculating propagation velocity. In the first case, one antenna remains stationary while the other is moved along the profile direction. In the second case, both antennas are simultaneously moved apart at the same speed on either side of the midpoint of the profile (Tillard and Jean-Claude, 1995). The measurement can also be achieved by using multi-offset method with multiple pair of antennae or one transmitter and multiple receivers.

Most of the GPR testing was carried out on actual railway lines (Brough et al., 2003; Carpenter et al., 2004; Eriksen et al., 2004). There are a lot of uncertainties within the actual rail track and it is difficult to calibrate the GPR data with actual ground condition because of a limited number of trenches and time constraint. Variation of degree of fouling also varies from site to site. In previous investigations limited attempt has been made to known degree of fouling and type of fouling using GPR testing on large scale model track. Leng and Al-Qadi(2010) carried out GPR survey on controlled model study in the laboratory and measured accurately the dielectric constants of two common ballast types, granite and limestone, under various fouling and moisture conditions. In order to investigate the relationship between recorded GPR data and ballast fouling conditions, a number of experiments are conducted on the model track with four different GPR frequencies.

5.1. Data and processing

Data were acquired using GPR with 500 MHz, 800 MHz, 1.6 GHz and 2.3 GHz ground coupled antennas. Wheel encoder was used to measure the traveling distance of the antennas over ballast surface. For the 500 MHz and 800 MHz antennas, an X3M control unit and an XV11 monitor were used to collect the data. For higher frequency antennas, a CX10 monitor with a control unit was used. During the testing, the antennas were placed on thin smooth plywood to prevent it from bouncing ballast surface. The horizontal sampling interval is 0.01 m while other acquisition parameters are different between antennas.

Raw data were processed using data processing software. The aim of this processing is to enhance signal–noise ratio and highlight interfaces and radargram textures. The processing includes band pass filtering, DC removal, subtract mean trace and gain control. Only very fundamental filters were applied to the raw data to avoid introducing artificial textures into the radargram. A comparison between raw and processed data from the 500 MHz antenna traveling along the left side of the track in the longitudinal direction is presented in Fig. 9. The depth in the radargram was calculated based on an estimated wave velocity of 1.1×10^8 m/s. From the raw data, two hyperbolas and two interfaces can be observed below the time of about 5 ns but no useful information can be obtained close to the ballast surface because of noise. After the above mentioned filters have been applied, an obvious improvement of the signal/noise ratio can be observed. The interface between ballast and capping layer is revealed at the time of about 5 ns. Differences between textures of radargram at different locations can be observed which can help us judge that the condition of the ballast is not uniform.

5.2. Results and discussion

The quality of GPR data that can be obtained is strongly correlated to the frequency of the antenna. Low frequency antenna can see deeper into the ground but gives lower resolution. On the contrary, high frequency antenna gives high resolution but can only penetrate through a shallower depth. For the specific application of monitoring ballast, the very high frequency antenna will pick up ballast particles and receive strong reflections from the voids between them. This makes it possible to evaluate ballast fouling condition by comparing the textures of the radargram. However, the strong reflection from ballast voids will also weaken the reflections from existing interfaces and/or objects and make it difficult to recognize them. Therefore antennas with four different frequencies were tested during the testing to find out an optimum frequency for monitoring the ballast condition.

Fig. 10 shows the processed GPR data for four antennas across the sections 1 to 9. The interfaces are marked out using dashed lines. The result of the 500 MHz antenna (Fig. 10a) shows the interfaces between ballast and capping layer, capping and subgrade and

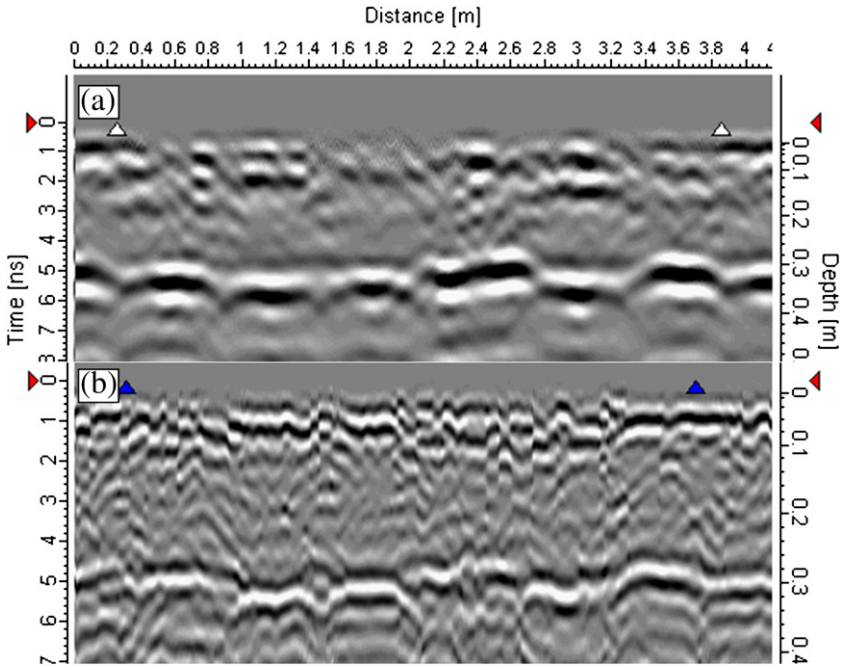

Fig. 11. Radargrams for (a) the 800 MHz and (b) 1.6 GHz antennas along line 1.

subgrade and concrete floor. Two hyperbolas reflected from two steel pipes with a diameter of 50 mm are also showed on the radargram. Different textures are observed from different sub-sections of the track, but they are not very clear due to low resolution of the antenna. The 800 MHz antenna (Fig. 10b) could also detect the interfaces and embedded steel pipes from the hyperbolae and different textures between clean and fouled sections were visible on the radargram. The textures of the clean sections (sections 6 and 8) were clearer than those of the adjacent fouled sections (such as section 7). Interfaces between different layers are also shown on the radargram of 1.6 GHz antenna (Fig. 10c), but the hyperbolas and difference of texture are not very clear. The reason for this might be the reflections from ballast particles. The 2.3 GHz antenna (Fig. 10d) only reveals the interface between the ballast and the capping layer because of its smaller depth of penetration. The comparison in Fig. 10 between the four radargrams shows that as the frequency increased the texture of the radargram became finer, but the ability to detect interfaces with the antenna decreased. Of the four frequencies tested here, the 800 MHz antenna gave the clearest image for monitoring the state of the track layers.

Although the radargram textures for the 800 MHz antenna show some difference between clean and fouled ballast, it is still difficult to identify the fouling just by visual inspection of the radargram. Further evaluation methods, such as calculating and comparing the dielectric permittivity or analyzing the amplitude or frequency spectra should be developed. Fig. 11 shows the radargrams from the 800 MHz and 1.6 GHz antennas traveling along line 1. As radar detectable Geotextile was embedded under the ballast along line 1, the interface between ballast and the capping layer is very prominent (Fig. 11a). It can be found that the recorded two-way travel times for the interface in different sub-sections are different. However, the depth of the interface is the same all along the line. Therefore it can be concluded that the propagation velocity of radar signal in different sub-sections is different, which is due to difference in fouling conditions. This indicates that it is possible to evaluate ballast fouling condition by measuring the propagation velocity of radar signal. GPR shows the interface (depth) of fouling layer but type of fouling may not be identified. GPR survey can be performed faster than seismic surface-wave survey. In an unknown field condition, direct application of GPR to measure degree and type of fouling has to be further investigated using a better signal processing.

6. Conclusions

Typical model track with clean and fouled ballast beds has been designed and constructed at the University of Wollongong. MASW and GPR surveyshave been conducted on model track to identify the degree of fouling and type of fouling. Seismic surface-wave survey shows that the shear wave velocity increases before optimum fouling point (OFP) and decreases after OFP. Coal fouled ballast bed reaches the OFP ahead of sandy clay fouled ballast bed. Coal fouled ballast bed has relatively higher shear strength before OFP but clay fouled ballast bed has relatively higher shear strength after the OFP. The shear wave velocity of fouled ballast decreases after OFP and goes below the clean ballast. Degree of fouling corresponding to shear wave velocity of fouled ballast equal to clean ballast is called as critical fouling point. The critical fouling point for sandy clay fouled ballast is 36% and coal fouled ballast is 39%.

GPR studies on model track show that the fouled layer can be identified using GPR but still degree of fouling and type of fouling are uncertain. Among 500 MHz, 800 MHz, 1.6 GHz and 2.3 GHz surface bound antenna, 800 MHz antenna gives relatively comparable results.

This study shows that seismic surface-wave survey can provide low strain shear wave velocity of ballast bed thereby enabling the identification of type and degree of fouling. This shear wave velocity can also be used to find low strain stiffness of substructure of the rail track. While, depth of fouling layer identification can be approximate in seismic reaction survey, radar gram from GPR shows interface of layer clearly. GPR results are qualitative and further calibration with actual track condition is needed.

Based on this study it can be concluded that MASW is the ideal tool for type of fouling identification. However concrete method need to be worked out to identify the degree of fouling based on shear wave velocity by considering model and field studies. The parabolic shape shear wave velocity variation shows two degree of fouling point for the same shear wave velocity i.e. before OFP and after OFP. MASW survey in the field may not be as fast as GPR survey. Considering limitations in model track when compared to field, it is further planned to conduct field model test using GPR as well as MASW to confirm the finding in the model track.

Acknowledgment

The first author thanks the Endeavor and Australian Government for being invited to be an Endeavor research fellow.

References

Aki, K., Richards, P.G., 1980. Quantitative Seismology. W.H. Freeman & Co.
Al-Hunaidi, M.O., 1992. Difficulties with phase spectrum unwrapping in spectral analysis of surface waves non-destructive testing of pavements. Can. Geotech. J 29, 506–511.
Anbazhagan, P., Sitharam, T.G., 2008a. Mapping of average shear wave velocity for Bangalore region: a case study. J. Environ. Eng. Geophysics 13 (2), 69–84.
Anbazhagan, P., Sitharam, T.G., 2008b. Seismic microzonation of Bangalore. J. Earth Syst. Sci. 117, No.S2, 833–852.
Anbazhagan, P., Sitharam, T.G., 2008c. Site characterization and site response studies using shear wave velocity. J. Seismology and Earthquake Eng. 10 (2), 53–67.
Anbazhagan, P., Sitharam, T.G., 2008d. Application of multichannel analysis of surface wave survey in geotechnical engineering problems. Proceeding of 6th Asian Young Geotechnical Engineers Conference, pp. 291–300.
Anbazhagan, P., Sitharam, T.G., 2009. Spatial variability of the weathered and engineering bed rock using multichannel analysis of surface wave survey. Pure and Applied Geophysics 166 (3), 409–428.
Anbazhagan, P., Indraratna, B., Rujikiatkamjorn, C., Su, L., 2010. Using a seismic survey to measure the shear modulus of clean and fouled ballast. Geomechanics and Geoengineering: An International Journal 5 (2), 117–126.
AS 2758.7, 1996. Australian standard: aggregates and rock for engineering purposes. Part 7: Railway Ballast. .
Effects of railroad track structural components and subgrade on damping and dissipation of train induced vibration. Doctoral Thesis. : Bei S.The Graduate School, University of Kentucky, Lexington, Kentucky, China.
Brough, M., Stirling, A., Ghataora, G., Madelin, K., 2003. Evaluation of railway track bed and formation: a case study. NDT&E International 36, 145–156.
Carpenter, D., Jackson, P.J., Jay, A., 2004. Enhancement of the GPR method of railway track bed investigation by the installation of radar detectable geosynthetics. NDT&E International 37, 95–103.
Clark, M.R., Gillespie, R., Kemp, T., McCann, D.M., Forde, M.C., 2001. Electromagnetic properties of railway ballast. NDT&E International 34, 305–311.
Daniels, D.J., 2004. Ground Penetrating Radar, 2nd ed. The Institution of Electrical Engierrs, Stevenage, UK.
Dorman, J., Ewing, M., 1962. Numerical inversion of seismic surface wave dispersion data and crust-mantle structure in the New York–Pennsylvania area. J. Geophys. Res. 67, 5227–5241.
Eriksen, A., Gascoyne, J., Al-Nuaimy, W., 2004. Improved productivity & reliability of ballast inspection using road-rail multi-channel GPR. 6th–7th July Proceedings of Railway Engineering. Commonwealth Institute, London, UK, pp. 1–5.
Feldman, F., Nissen, D., 2002. Alternative Testing Method for the Measurement of Ballast Fouling: Percentage Void Contamination. Conference on Railway Engineering, Wollongong, RTSA. pp. 101–109.
Gallaghera, G.P., Leiper, Q., Williamson, R., Clark, M.R., Forde, M.C., 1999. The application of time domain ground penetrating radar to evaluate railway track ballast. NDT&E International V32, 463–468.
Ganji, V., Gukunski, N., Maher, A., 1997. Detection of underground obstacles by SASW method—numerical aspects. J. Geotech. Geoenviron. Eng. 123 (3), 212–219.
Indraratna, B., Su, L., Rujikiatkamjorn, C., 2011. A new parameter for classification and evaluation of railway ballast fouling, Technical note. Can. Geotech. J. 48, 322–326.
Leng, Z., Al-Qadi, I.L., 2010. Railroad ballast evaluation using ground penetrating radar. January 10–14 Laboratory Investigation and Field Validation. Transportation Research Board 89th Annual Meeting, Washington, D.C, pp. 1–15.
Mari, J.L., 1984. Estimation of static correction for shear-wave profiling using the dispersion properties of Love waves. Geophysics 49, 1169–1179.
Nazarian, S., Stokoe II, K.H., Hudson, W.R., 1983. Use of spectral analysis of surface waves method for determination of moduli and thicknesses of pavement systems. Transp. Res. Rec 930, 38–45.

Park, C.B., Miller, R.D., Xia, J., 1999. Multi-channel analysis of surface waves. Geophysics 64 (3), 800–808.
Press, W.H., Teukosky, S.A., Vetterling, W.T., Flannery, B.P., 1992. Numerical Recipes in C: Cambridge Univ. Press.
Schwab, F.A., Knopoff, L., 1972. Fast surface wave and free mode computations. In: Bolt, B.A. (Ed.), Methods in Computational Physics. Academic Press, pp. 87–180.
Selig, E.T., Waters, J.M., 1994. Track geotechnology and substructure management, London. Thomas Telford, New York, American Society of Civil Engineers. Publications Sales Dept.
Sitharam, T.G., Anbazhagan, P., 2008. Evaluation of Low strain dynamic properties using geophysical method: a case study. Consulting Ahead 2 (2), 34–50.
Stokoe II, K.H., Wright, G.W., James, A.B., Jose, M.R., 1994. Characterization of geotechnical sites by SASW method. In: Woods, R.D. (Ed.), Geophysical Characterization of Sites: ISSMFE Technical Committee #10. Oxford Publishers, New Delhi.
Sussmanna, T.R., Ernest, T., Selig, J., Hyslip, P., 2003. Railway track condition indicators from ground penetrating radar. NDT&E International 36, 157–167.
Tillard, S., Jean-Claude, D., 1995. Analysis of GPR data: wave propagation velocity determination. J. Appl. Geophysics 33, 77–91.
Tokimatsu, K., 1995. Geotechnical site characterization using surface waves IS-Tokyo Proc. 1st Int. Conf. on Earth. Geotechn. Eng. 36.
Xia, J., Miller, R.D., Park, C.B., 1999. Estimation of near-surface shear-wave velocity by inversion of Rayleigh wave. Geophysics 64 (3), 691–700.
Xu, Y., Xia, J., Miller, R.D., 2006. Quantitative estimation of minimum offset for multichannel surface-wave survey with actively exciting source. J. Appl. Geophysics 59 (2), 117–125.
Zhang, S.X., Chan, L.S., Xia, J., 2004. The selection of field acquisition parameters for dispersion images from multichannel surface wave data. Pure and Appl. Geophysics 161, 185–201.